Direct inelastic scattering of N_2 from Ag(111). III. Normal incident N_2

Andrew C. Kummel, Greg O. Sitz, and Richard N. Zare
Department of Chemistry, Stanford University, Stanford, California 94305

John C. Tully
AT&T Bell Laboratories, Murray Hill, New Jersey 07974

(Received 12 July 1988; accepted 23 August 1988)

We have probed the angular momentum orientation of N_2 scattered from cold Ag(111) when the N_2 approaches the surface along the surface normal. Using resonance enhanced multiphoton ionization (REMPI) and pulsed molecular beam techniques, we are able to probe the flux backscattered along the surface normal. In accordance with the restrictions on cylindrically symmetric systems, the molecules backscattered along the surface normal have no angular momentum orientation nor does the entire scattered flux integrated over all exit angles. However, for detection away from the surface normal, we observe substantial angular momentum orientation; the degree and direction of orientation depends upon the rotational state being probed. Molecular dynamics calculations reproduce the experimental results semiquantitatively. The calculations show that for N_2 incident along the surface normal, the exit angle is largely determined by the two-dimensional impact parameter of the molecule within the crystal unit mesh. However, the final rotational state, orientation, and alignment are determined largely by the molecular orientation geometry of the N_2 during the collision. In essence, we have found a dynamical process which can partially differentiate between the two hidden initial conditions in a gas–surface collision: the two-dimensaional impact parameter and the molecular orientation geometry.

I. INTRODUCTION

For measurements on monoenergetic molecular beams directly scattered from cold ($T_s < T_{\text{Debye}}$) single crystals, the observables may be classically pictured as averages over two initial conditions: the molecular orientation geometry of the molecule prior to collision and the two-dimensional impact parameter. By molecular orientation geometry we mean the instantaneous direction of the bond axis (or figure axis) of the molecule with respect to the crystal lattice. The two-dimensional impact parameter refers to the projection of the incident velocity vector of the center of mass of the gas molecule onto the crystal unit mesh. For a corrugated, hard wall, repulsive model of the gas–surface collision, the molecular orientation geometry refers to the position of the bond axis at the turning point of the molecule's translational motion, and the two-dimensional impact parameter is equivalent to the contact point between the molecule and the crystal lattice. By carrying out normal incidence scattering of N_2 from cold Ag(111) in which the scattered N_2 is state selectively detected and the angular momentum polarization is measured as a function of exit angle, we show that these averages over molecular orientation geometry and two-dimensional impact parameter may be partially disentangled.

The angular momentum polarization can be divided into two types: alignment and orientation. Alignment refers to preferential occupation of sublevels M_z and $-M_z$ as opposed to M_z' and $-M_z'$ for molecules in a given J state; this is equivalent to the molecules in state J having a preferred plane of rotation. Orientation refers to preferential occupation of sublevel $+M_z$ as opposed to sublevel $-M_z$ (clockwise vs counterclockwise rotation) for molecules in a given J state; oriented molecules in state J always have a preferred direction of rotation and usually have a preferred plane of rotation.

Since molecular orientation geometry refers to the instantaneous direction of the bond axis (or figure axis) of the molecule with respect to the crystal unit mesh, the molecular orientation geometry changes as the molecule rotates. In the experiments described here, some of the N_2 molecules impinging on Ag(111) were populated in rotational levels $J = 1$ and 2. However, the rotational periods of these states are long (~ 3 ps) compared to the duration of the collision (~ 0.1 ps). Hence, from the perspective of the surface, the molecule approaches with an almost fixed molecular orientation geometry which may be changed only by the attractive and repulsive forces acting during the collision. This is a classical picture, but there is a quantum mechanical analog.

For a $^1\Sigma$ diatomic molecule in a $|JM\rangle$ state in a field-free region, we cannot know its molecular orientation geometry because this requires knowledge of $\langle|J|\rangle$ and its conjugate variable $\langle|\phi_J|\rangle$ (the angle/phase of the rotation). However, in the presence of a strong field (such as a Stark field), the wave functions for neighboring J states become mixed, and we can have knowledge of the molecular orientation geometry because its conjugate variable $\langle|J|\rangle$ is no longer well-defined. Analogously, when a molecule hits the surface, the fields are very strong, so that during the collision, $\langle|J|\rangle$ is not well-defined, but the molecular orientation geometry can be sensed. In fact, it is the mixing of J states during the collision which allows rotational excitation to occur during the collision. This is not to say that we can measure the molecular orientation geometry during the collision, but rather that the molecular orientation geometry can be properly thought of as one of the initial conditions which

determines the final quantum state, polarization, and exit angle.

For internally cold molecules incident upon a cold surface at a given incident angle and energy, the important initial conditions are the molecular orientation and the two-dimensional impact parameter. For "glancing" incident N_2/Ag(111) scattering ($\theta_i = 30°$), we have made extensive measurements of (1) the population, (2) the velocity distributions, (3) the alignment, and (4) the orientation as a function of the rotational quantum number of scattered molecules.[1–4] The polarization of direct inelastically scattered molecules has been recorded for a few other systems: NO/Ag(111),[5] NO/Pt(111),[6] CHF_3/Ag(111),[7] and NH_3/Au(111).[8] For the NH_3 experiments, the projection of the angular momentum **J** onto the figure axis of the molecules was measured (quantum number K in the $|JMK\rangle$ basis set) rather than the projection of **J** onto a space fixed axis (quantum number M). For the CHF_3 experiments, the products of quantum numbers K and M were measured (heads vs tails).

The results for N_2/Ag(111) suggest that the molecular orientation geometry and the two-dimensional impact parameter are the important initial conditions.[4] However, for glancing incidence, it is difficult to differentiate experimentally between the effects of these two initial conditions. For normal incidence experiments on N_2 scattering from cold Ag(111), we will demonstrate that the two-dimensional impact parameter is the dominant initial condition in determining the exit angle, while the molecular orientation geometry before the collision is the dominant initial condition in determining the rotational state and angular momentum alignment and orientation of the scattered molecules.

II. EXPERIMENT

The details of the experiment have been described elsewhere[3] but will be reviewed here with special attention to those features which enable normal-incidence normal-detection experiments to be performed.

The molecular beam is formed by expanding a mixture of 20% N_2 in H_2 through a 0.4 mm pulsed valve (General Valve Series 9). The beam is skimmed and then chopped in a separate chamber at 200 Hz (TRW 75A1003-2). The chopping speed is increased to 300 Hz for the velocity distribution measurements; this produces 12 μs pulses. The beam is collimated in a third chamber before entering the fourth, high vacuum, chamber. The high vacuum chamber has a base pressure of $3–4\times10^{-10}$ Torr, and the chopped beam raises this by less than 2×10^{-11} Torr.

The surface is a Ag(111) sample (Aremco Inc.) which is prepared by the standard techniques and brazed onto a copper support. In vacuum, the surface is cleaned by argon ion sputtering and then annealed. The surface cleanliness and order are checked using Auger and LEED spectroscopies. When experiments are being performed, the surface is maintained at 90 K but flashed to 700 K every 30–45 min in order to preserve surface cleanliness. The surface is positioned so that the surface normal lies along the molecular beam axis (see Fig. 1).

The N_2 is state-selectively detected using a 2 + 2 resonantly enhanced multiphoton ionization of the $a\ ^1\Pi_g$–$X\ ^1\Sigma_g^+$ (1,0) transition. The 283–285 nm radiation is generated by frequency doubling the output of a Nd^{+3}:YAG pumped dye laser (Qauntel YGC581C-TDL50-UVX2). A rhodamine 590/610 dye mix (7:1) is employed to give very small power variation across the spectroscopic band. The doubled and undoubled lights are separated using dichroic mirrors (CVI). The pure doubled light (13–16 mJ/pulse) is focused with a 20 cm AR coated lens into the scattered flux. The ions are collected in a time-of-flight tube which acts as a mass spectrometer and separates the reasonantly ionized N_2 from the nonresonantly ionized background.

The focusing lens is mounted 1 cm off the center line of a rotating mount, the axis of which is parallel to the front face of the Ag(111) crystal. The crystal is positioned so that the [211] azimuth is perpendicular to the laser propagation direction. When the lens is positioned so that the focus lies along the surface normal, we can time the firing of the laser so that we can ionize either the incident beam or the scattered flux (see Fig. 1); these signals are separated by $\sim$25 μs. By rotating the lens away from the surface normal, we can detect the off-specular scattered flux for normal incident molecules (see Fig. 1). The time-of-flight tube is perpendicular to the surface normal; hence, we can extract ions at specular and off-specular angles. The position of the laser focus determines the exit angle being probed.

To make the orientation measurements, the ellipticity (β) of the probe light must be varied while keeping a constant angle (Δ) between the surface normal and the major axis of polarization. In these experiments, the major axis of polarization is along the surface normal ($\Delta = 0°$). The ellipticity of the polarization is prepared using two optics. First, the laser beam passes through a half-wave plate (Special Optics) which rotates the linear polarized light (99.8%). The half-wave plate is in a precision mount (Oriel) which can be rotated by a stepper motor. Second, the light beam passes through a quarter-wave plate (Special Optics) whose optic axis is fixed along the surface normal.

III. RESULTS

A. Orientation vs exit angle

To measure the orientation, the ellipticity is fixed and the laser is scanned over a single rotational transition from ground state J_i to resonant state J_f. Then the ellipticity is changed, and the laser is scanned again across the same transition. The ellipticity β is changed so that measurements at $+\beta$ and $-\beta$ are taken consecutively. The intensity across the rotational transition at each β is integrated; the integrated intensities are labeled $I(J_i,J_f,\beta)$. The orientations can then be extracted using the formulas of Ref. 9:

$$\begin{aligned} I(J_i,J_f,\beta) = {} & a_{0+}^{\{0\}}(J_i,J_f)(\text{app})P_{0+}^{\{0\}}(J_i,J_f,\beta) + a_{1-}^{\{1\}}(J_i,J_f)(\text{app})P_{1-}^{\{1\}}(J_i,J_f,\beta) \\ & + a_{0+}^{\{2\}}(J_i,J_f)(\text{app})P_{0+}^{\{2\}}(J_i,J_f,\beta) + a_{1-}^{\{3\}}(J_i,J_f)(\text{app})P_{1-}^{\{3\}}(J_i,J_f,\beta) \\ & + a_{3-}^{\{3\}}(J_i,J_f)(\text{app})P_{3-}^{\{3\}}(J_i,J_f,\beta) + a_{0+}^{\{4\}}(J_i,J_f)(\text{app})P_{0+}^{\{4\}}(J_i,J_f,\beta), \end{aligned} \quad (1)$$

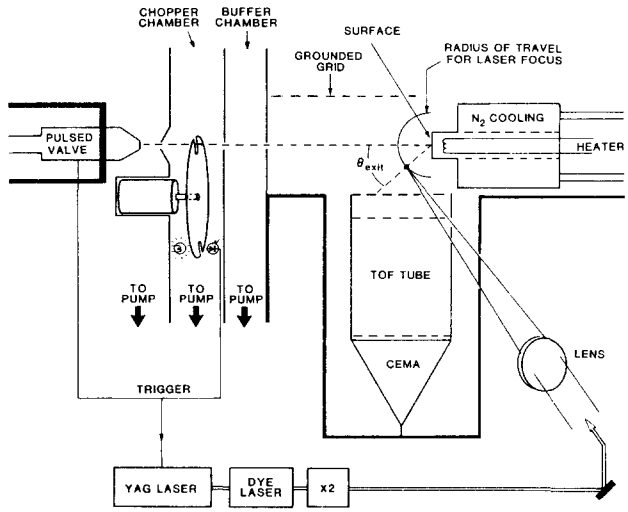

FIG. 1. Schematic diagram of the apparatus showing the normal-incidence normal-detection experiment. The angle of the surface is adjusted so that the incident molecular beam lies along the surface normal. The laser beam is focused by a lens placed on a rotary mount. The focal point is 1 cm from the surface, but the axis of the rotary mount is parallel to the surface plane. Hence, the focus can be rotated along a 1 cm radius whose centroid is the intersection of the molecular beam with the surface.

where

$$A^{\{k\}}_{q\pm}(J_i,J_f)(\text{app})/A^{\{0\}}_{0+}(J_i,J_f)(\text{app}) = a^{\{k\}}_{q\pm}(J_i,J_f)(\text{app})/a^{\{0\}}_{0+}(J_i,J_f)(\text{app}). \quad (2)$$

Here, the $a^{\{k\}}_{q\pm}$ are the unreduced apparent moments and the $P^{\{k\}}_{q\pm}$ are the corresponding moments of the line strength. The $P^{\{k\}}_{q\pm}$ are calculated using the equations of Ref. 9, while the $a^{\{k\}}_{q\pm}$ are determined by using a linear least squares fit of Eq. (1) to the data.

The real moments $A^{\{k\}}_{q\pm}(J_i)$ are just the expectation values of the angular momentum operators J_x, J_y, J_z. The apparent moments $A^{\{k\}}_{q\pm}(J_i,J_f)(\text{app})$ are sums of these real moments; the definitions of the apparent moments in terms of the real moments are specific to each rotational branch and each J_i. These are given in Table I. With our experimental geometry, the apparent moments for $A^{\{k\}}_{q\pm}$ with $k = 1,3$ are identical to the real moments:

$$A^{\{1\}}_{1-}(J_i,J_f)(\text{app}) = A^{\{1\}}_{1-}(J_i) = \langle (J_i|J_y/\mathbf{J}|J_i)\rangle, \quad (3a)$$

$$A^{\{3\}}_{1-}(J_i,J_f)(\text{app}) = A^{\{3\}}_{1-}(J_i) = [(2/3)^{1/2}/4] \times \langle [J_i|(J_{yz^2} - 3J_{y^3} - J_{x^2y})/\mathbf{J}^3|J_i]\rangle = \{[(6)^{1/2}/4][\langle J_i|J_y(5J_{z^2} - J^2)/\mathbf{J}^3|J_i]\rangle\}_{J\to\infty}, \quad (3b)$$

$$A^{\{3\}}_{3-}(J_i,J_f)(\text{app}) = A^{\{3\}}_{3-}(J_i) = [(10)^{1/2}/4]\langle [J_i|(J_{yx^2} - J_{y^3})/\mathbf{J}^3|J_i]\rangle = \{[(10)^{1/2}/4][\langle J_i|J_y(3J_{x^2} - J_{y^2})/\mathbf{J}^3|\mathbf{J}_i]\rangle\}_{J\to\infty}. \quad (3c)$$

The benefit of our being able to measure directly the $A^{\{k\}}_{q\pm}$ with $k = 1,3$ is realized only when we use both the O and P branches originating from the same J_i to determine the orientation. This allows us to differentiate between $A^{\{1\}}_{1-}$, $A^{\{3\}}_{1-}$, and $A^{\{3\}}_{3-}$. In all cases the fits of Eq. (1) to the data had smaller standard deviations when the $A^{\{3\}}_{3-}$ was set to zero. This is not unreasonable because the $P^{\{3\}}_{3-}$ line strength is small and has a variation with β similar to that of $P^{\{3\}}_{1-}$.

Once we assume that $A^{\{3\}}_{3-} = 0$, it is easy to fit jointly the data from $I(O\text{ branch}, J_i)$ vs β and $I(P\text{ branch}, J_i)$ vs β to determine $A^{\{1\}}_{1-}$ and $A^{\{3\}}_{1-}$. However, in the limit that $\langle (J_i|J_z/\mathbf{J}|J_i)\rangle = 0$, $A^{\{3\}}_{1-}(J_i) = 0.61A^{\{1\}}_{1-}(J_i)$ for large J_i [see Eqs. (3a) and (3b)]. This was checked experimentally by using Eq. (1) to fit the measurements of $I(J_i,J_f)$ vs β for both O and P branches for selected values of J (see Table II). For all other measurements, we assumed that $A^{\{3\}}_{1-}(J_i)/A^{\{1\}}_{1-}(J_i) = 0.61$.

For $J_i = 18$ and $J_i = 15$, the orientation was determined as a function of the exit angle θ_{exit}; Fig. 2 depicts the data for $J_i = 18$. While no orientation is observed for molecules backscattered along the surface normal ($\theta_{\text{exit}} = 0°$),

TABLE I. The apparent moments as a function of the reduced moments of the ground state distribution for $J = 20$ for N_2 undergoing the $a\,^1\Sigma_g^+ - X\,^1\Pi_g$ transition for $\phi = 0°$.

$A^{\{0\}}_{0+}(\text{app}) = A^{\{0\}}_{0+} - 0.781A^{\{2\}}_{2+} - 0.076A^{\{4\}}_{2+} + 0.201A^{\{4\}}_{4+}$	(P branch)
$A^{\{0\}}_{0+}(\text{app}) = A^{\{0\}}_{0+} + 0.279A^{\{2\}}_{2+} + 0.268A^{\{4\}}_{2+} - 0.709A^{\{4\}}_{4+}$	(O branch)
$A^{\{2\}}_{0+}(\text{app}) = A^{\{2\}}_{0+} - 0.247A^{\{2\}}_{2+} - 0.361A^{\{4\}}_{2+} + 0.382A^{\{4\}}_{4+}$	(P branch)
$A^{\{2\}}_{0+}(\text{app}) = A^{\{2\}}_{0+} - 0.247A^{\{2\}}_{2+} - 3.562A^{\{4\}}_{2+} + 3.770A^{\{4\}}_{4+}$	(O branch)
$A^{\{4\}}_{0+}(\text{app}) = A^{\{4\}}_{0+} + 1.168A^{\{2\}}_{2+} - 0.383A^{\{4\}}_{2+} + 0.169A^{\{4\}}_{4+}$	(P branch)
$A^{\{4\}}_{0+}(\text{app}) = A^{\{4\}}_{0+} + 0.118A^{\{2\}}_{2+} - 0.383A^{\{4\}}_{2+} + 0.169A^{\{4\}}_{4+}$	(O branch)
$A^{\{1\}}_{1-}(\text{app}) = A^{\{1\}}_{1-}$	(P branch)
$A^{\{1\}}_{1-}(\text{app}) = A^{\{1\}}_{1-}$	(O branch)
$A^{\{3\}}_{1-}(\text{app}) = A^{\{3\}}_{1-}$	(P branch)
$A^{\{3\}}_{1-}(\text{app}) = A^{\{3\}}_{1-}$	(O branch)
$A^{\{3\}}_{3-}(\text{app}) = A^{\{3\}}_{3-}$	(P branch)
$A^{\{3\}}_{3-}(\text{app}) = A^{\{3\}}_{3-}$	(O branch)

TABLE II. Comparison of $A_1^{\{1\}}(J_i)$ with $A_{1-}^{\{3\}}$. Conditions: $\theta_i = 0°$, $E_i = 0.3$ eV, $T_s = 90$ K.

J	θ_{exit}	$A_1^{\{1\}}$	$A_{1-}^{\{3\}}$	$A_{1-}^{\{3\}}/A_{1-}^{\{1\}}$
18	$-20°$	-0.17 (0.03)	0.10 (0.07)	-0.59 (0.52)
18	$+15°$	0.15 (0.04)	-0.11 (0.08)	-0.73 (0.73)
11	$+20°$	0.12 (0.03)	-0.074 (0.041)	-0.62 (0.50)
16	$+20°$	0.34 (0.02)	-0.18 (0.04)	-0.53 (0.15)
18	$+20°$	0.15 (0.04)	-0.11 (0.08)	-0.73 (0.73)

$[A_{1-}^{\{3\}}/A_{1-}^{\{1\}}]_{av} = -0.64$

$[A_{1-}^{\{3\}}/A_1^{\{1\}}]_{\langle Jz\rangle = 0} = -0.61$

there is increasing orientation away from the surface normal. The orientation is asymmetric about $\theta_{exit} = 0°$, that is, $A_{1-}^{\{1\}}(J_i,\theta_{exit}) = -A_{1-}^{\{1\}}(J_i,-\theta_{exit})$; this was not observed for experiments done with glancing incident N_2. This means that for normal incident N_2, the total scattered flux has no orientation:

$$\int_{-\pi/2}^{\pi/2} A_{1-}^{\{1\}}(J_i,\theta_{exit})\,d\theta_{exit} = 0.$$

These two observations, $A_{1-}^{\{1\}}(J_i,\theta_{exit} = 0°) = 0$ and $A_{1-}^{\{1\}}(J_i,\theta_{exit})\,d\theta_{exit} = 0$ (see Fig. 2) confirm that the rules governing cylindrical symmetry for normal incidence scattering are being obeyed. Even though the surface is not flat, it has sixfold symmetry. As long as the surface is not chiral, the backscattered molecules (the ones detected along the surface normal) cannot be oriented. Since the surface is positioned so that the detection plane lies along a symmetry axis, the molecules being scattered upwards ($\theta_{exit} > 0°$) have the same alignment and orientation of the same magnitude but opposite sign, as the molecules scattered downward ($\theta_{exit} < 0°$) (see Fig. 1). Our data show that the orientation is approximately a linear function of the exit angle; this is specific to the N_2/Ag(111) system and not required by the rules governing cylindrical symmetry.

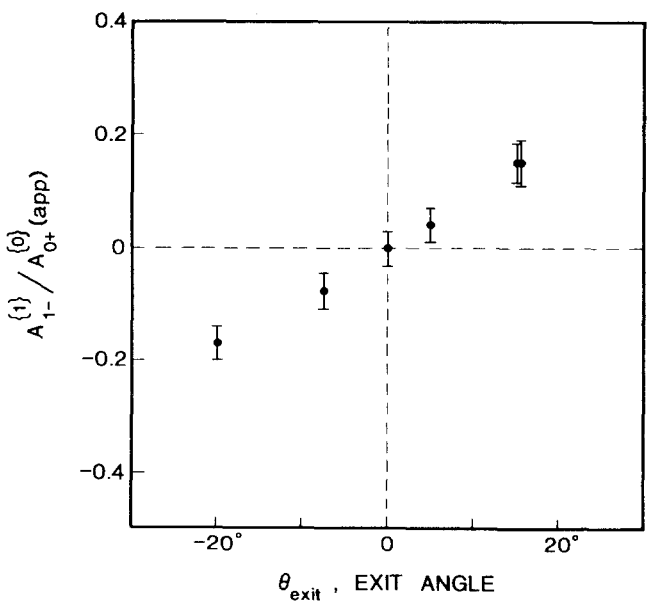

FIG. 2. $A_1^{\{1\}}(J_i = 18, J_f = 20)$ vs θ_{exit} for $E_i = 0.3$ eV, $T_s = 90$ K, and $\theta_i = 0°$.

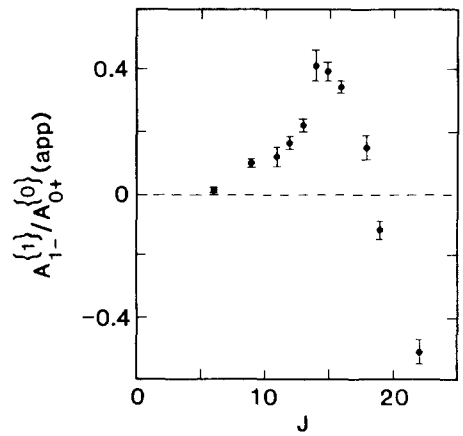

FIG. 3. $A_{1-}^{\{1\}}$ vs J_i for $E_i = 0.3$ eV, $T_s = 90$ K, $\theta_i = 0°$, and $\theta_{exit} = +15°$.

B. Orientation vs J

At a fixed exit angle, $\theta_{exit} = +15°$, the orientation was measured as a function of J_i (see Fig. 3). These data look quite similar to our previously reported experiments on glancing incidence N_2 off Ag(111) with detection along the quasi-specular direction. The orientation is strongest for the highest J state; switches sign at about $J = 17$; peaks for the intermediate J states (the ones on the low energy side of the rainbow); and gradually decreases at low J.

A simple model may be used to interpret the data. For a sphere hitting a hard corrugated surface, the exit angle is determined by the two-dimensional impact parameter (see Fig. 4). Since the N_2 molecule appears to the surface to be a nearly spherical ellipsoid, the dominant initial condition in determining the exit angle of N_2 scattering off a hard corrugated surface is the two-dimensional impact parameter. Of course, the molecular orientation geometry does influence the exit angle, but for nearly spherical ellipsoids (as opposed to a stick), this is a less important initial condition. This assertion will be reinforced by the calculations reported in the next section. In order to construct a simple picture of orientation vs J at a fixed exit angle, let us first consider only trajectories with the two-dimensional impact parameter shown in Fig. 5. We assume that the impact parameter chosen for Fig. 5 results in scattering to a positive exit angle.

For an ellipsoid hitting a hard corrugated surface with a given two-dimensional impact parameter, the final J states and orientations are greatly influenced by the molecular geometry. Let us imagine a set of local coordinates (x_L, y_L, z_L)

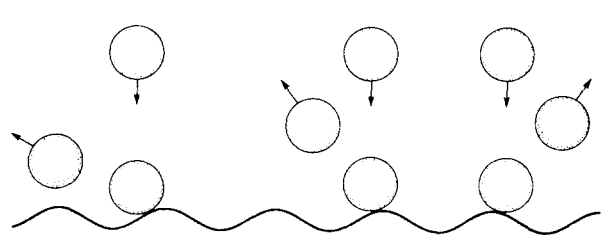

FIG. 4. Ellipsoids scattering off a hard corrugated surface showing exit angle vs two-dimensional impact parameter.

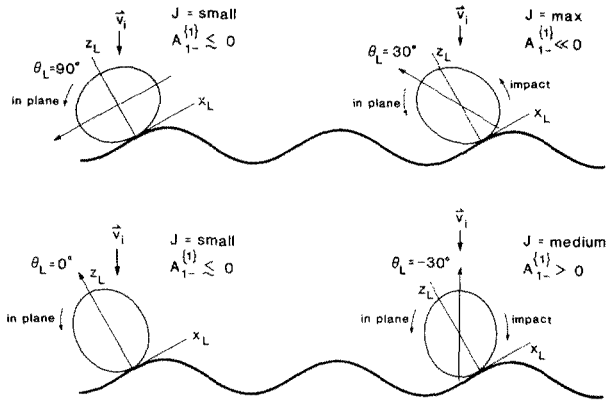

FIG. 5. Ellipsoids scattering off a hard corrugated surface for a particular two-dimensional impact parameter but with different molecular orientation geometries. Initially, the ellipsoids are nonrotating and are directed along the overall surface normal. Shown is the variation in the magnitude and orientation of **J** with θ_L, the angle between the local surface normal z_L and the major axis of the ellipsoid.

for which z_L is perpendicular to the surface tangent at our projected point of impact for the N_2 molecule, i.e., z_L is the "local normal." The propagation direction of the laser is designated as y_L, and this fixes x_L (see Fig. 5). This is a simple extension of our previously proposed ellipsoid/frictional surface model[4] with one difference; here, the normal and tangential momenta are defined with respect to the local normal at the collisional impact site.

Let us consider first only those molecules whose bond axes lie in the scattering plane, $\theta_L = 0°$, since these are the molecules which are most likely to scatter into the detection plane. In Fig. 5, $\theta_L = 0°$ corresponds to the plane of the figure. Let us designate θ_L as the angle between the bond axis and the local surface normal z_L. The final rotational state and orientation are now solely a function of θ_L since the two-dimensional impact parameter and θ_L are fixed and the surface is assumed to be motionless and the ellipsoid is assumed to be initially not rotating.

Our previous model[4] assumed a friction-like in-plane force. It would predict a zero net orientation for a normal incidence beam because it averaged over all impact sites. Our new model also predicts zero net orientation if we average over all impact sites. However, for a given impact site, net orientation can result from two sources: (1) correlations between initial conditions, and (2) inelastic or dissipative forces. Consider the first mechanism. At a given impact site the molecular orientations are not uniformly distributed because all elements on the ellipsoid surface do not strike a given impact site with equal probability. For example, in Fig. 5 there may be more molecules with $\theta_L = 30°$ than with $\theta_L = -30°$; this is most pronounced for glancing incidence experiments or for impact sites close to the "hollows." For normal incidence with impact sites close to the "atop" positions, this should be a small effect.

Consider the second mechanism for production of net orientation, inelastic, or dissipative forces. The corrugated surface can exert two types of forces which cause rotational excitation: the "impact" force and the "in-plane" (x_L, y_L) force. The impact force is just the restoring force of the surface in the z_L direction; this causes local specular scattering for incoming spheres. The second force is a resistance to motion in the x_L and y_L directions. Because the N_2 molecule is about half the size of the lattice spacing and because the potential has a steep gradient, the surface can exert different forces on the two atoms which are analogous to the in-plane forces (x_L, y_L) which our corrugated surface can exert on the ellipsoid.

For an ellipsoid colliding with the impact parameter depicted in Fig. 5 and with a molecular geometry such that its major axis is either parallel or perpendicular to z_L ($\theta_L = 0°$ or 90°), the impact does not cause rotational excitation, but local in-plane forces (x_L, y_L) may cause a small amount of counterclockwise rotation [$A^{\{1\}}_{1-}$ (small J) $\lesssim 0$]. If the molecular orientation is such that $\theta_L = \pm 30°$, the impact causes substantial clockwise ($\theta_L > 0°$) or counterclockwise ($\theta_L < 0°$) orientation. However, the in-plane forces always act to give counterclockwise orientation. Hence, the molecules with $\theta_L \simeq +30°$ leave the surface with $A^{\{1\}}_{1-}$ (large J) $\ll 0$, whereas the molecules with $\theta_L \simeq -30°$ leave the surface with $A^{\{1\}}_{1-}$ (medium J) > 0. At small J, we see a mixture between the low energy tail of the rotational rainbow for $\theta_L \simeq 90°$ (clockwise rotation) and the molecules with $\theta_L \simeq 0°$ (counterclockwise rotation). Consequently, the molecules at small J should have almost no net orientation [$A^{\{1\}}_{1-}$ (small J) $\simeq 0$]. These predictions from this simple model explain the trends in the data in Fig. 3: $A^{\{1\}}_{1-}$ (large J) $\ll 0$, $A^{\{1\}}_{1-}$ (medium J) > 0, and $A^{\{1\}}_{1-}$ (small J) $\simeq 0$. These trends are also seen in the trajectory calculations described in the next section.

C. Velocity vs orientation

Using the methods described previously,[3] the delay between the firing of the laser and the opening of the chopper was varied in order to measure the velocity distribution of the molecules scattered off the surface. For $J_i = 16$, the velocity distribution was measured with left circularly polarized light and with right circularly polarized light (see Fig. 3). For O branch excitation ($\Delta J = -2$), when left circularly polarized light is being employed, the molecules which are rotating counterclockwise are preferentially excited and ionized. Conversely, when right circularly polarized light is being employed, the molecules which are rotating clockwise are preferentially excited and ionized. In this fashion, we obtain a measure of the relative velocities of the molecules rotating clockwise vs counterclockwise by comparing time-of-flight (TOF) data for the two opposite polarizations.

The TOF distributions were recorded for $J_i = 16$ since this was one of the most strongly oriented rotational states. For the $\theta_{\text{exit}} = +15°$, $A^{\{1\}}_{1-}$ ($J_i = 16$) $= +0.34$; hence, clockwise rotation is preferred. The velocity distributions show that for $J_i = 16$ at $\theta_{\text{exit}} = +15°$, the molecules ionized with left circularly polarized light (counterclockwise rotating molecules) have, on average, a velocity $10 \pm 2.5\%$ larger than those ionized with right circularly polarized light (clockwise rotating molecules).

The results can be interpreted using the ellipsoid model described above. Looking at Fig. 5, we see that the molecules

with $\theta_L = 25°$ should have about the same final J state as molecules with $\theta_L = -30°$ because the molecules with positive θ_L do not need to overcome in-plane forces in order to scatter into a high rotational state. For scattering into positive exit angles by molecules with negative θ_L, the in-plane forces impart a counterclockwise torque, and thus the impact forces must exert an even larger clockwise torque in order to scatter the molecules into a high clockwise rotational state. Since these trajectories with negative θ_L are inefficient at net clockwise rotational excitation, they leave the surface with less translational energy than molecules in the same J state which are rotating counterclockwise (positive θ_L).

The simple model of ellipsoids hitting corrugated surfaces is a gross oversimplification of the N_2/Ag(111) system, but it does provide a zero-order interpretation of the data. For a more quantitative picture, we have carried out stochastic trajectory simulations which are described in the next section.

IV. STOCHASTIC TRAJECTORY CALCULATIONS

We have carried out stochastic trajectory calculations of normal incidence scattering of N_2 from Ag(111), following techniques described elsewhere.[10] The calculations reproduce the experimental results with reasonable accuracy. They also clarify the origin of the observed rotational orientation. The calculations demonstrate the extent to which the effects of the two dominant initial conditions, the molecular orientation geometry and the two-dimensional impact parameter, can be experimentally differentiated in normal incidence scattering. Details of the calculational methodology are given in the Appendix.

An empirical interaction potential was employed which acceptably reproduces the experimental measurements of final angular momentum as well as final alignment and orientation moments for a variety of incident N_2 velocities and angles and Ag(111) surface temperatures.[11] The calculations successfully track our experimentally observed trends for normal incidence scattering. For example, Fig. 6 shows the calculated variation of $A_{1-}^{\{1\}}$ vs final scattering angle for $E_i = 0.3$ eV, $T_s = 90$ K, $T_{\rm rot}$(init) $= 0$ K, and $\theta_i = 0°$. These calculations are in agreement with the experimental results in Fig. 2, within the uncertainties of the experimental and calculated points. Figure 7 shows calculated $A_{1-}^{\{1\}}$ ($\theta_f = 12°$ to 15°) vs final J for the same conditions as Fig. 6. These calculated moments are in accord with the corresponding experimental results of Fig. 3. In particular, the calculation reproduces the region of "backspin" (positive $A_{1-}^{\{1\}}$) in the vicinity of $J = 15$.

The satisfactory agreement with experiment lends credence to the validity of the stochastic calculations and to the assumed gas–surface interaction potential. Thus, we are relatively confident in drawing qualitative insights into the collison dynamics from examination of the computed trajectories. We conclude that the in-plane forces that are required to produce the experimentally observed orientation are present on a flat clean surface; defects, steps, or impurities are not required for this effect. Secondly, a "conduction electron drag" effect is also not required. Although we cannot demonstrate that conduction electron drag does not contribute, we do know that it is not the dominant factor. The calculated rotational orientation arises entirely from corrugation in the gas–surface interaction potential and is of comparable magnitude to that observed experimentally. Therefore, we conclude that this corrugation is the dominant source of the in-plane forces which gives rise to the experimental observations.

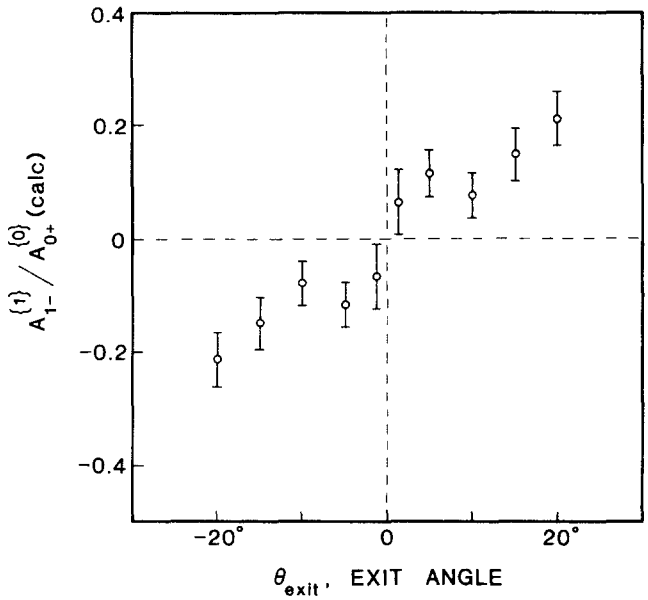

FIG. 6. Calculated $A_1^{\{1\}}$ ($J_i = 18$–$21, J_{avg} = 19.3$) vs θ_{exit} for $E_i = 0.3$ eV, $T_s = 90$ K, T_{rot}(init) $= 0$ K, and $\theta_i = 0°$. The exit angles were binned as follows (0.0–2.5, 2.5–7.5, . . . , 22.5–27.5). Symmetry has been used to improve statistics; the calculations are constrained to be antisymmetric with respect to $\theta_{exit} = 0°$. The error bars denote one standard deviation.

Information concerning the correlation between initial conditions and final scattering properties is displayed in Fig. 8. Four final-state properties of the ensemble of scattered molecules are plotted as a function of two initial conditions, the molecular orientation geometry and the two-dimensional impact parameter. A sample of 5000 trajectories was run

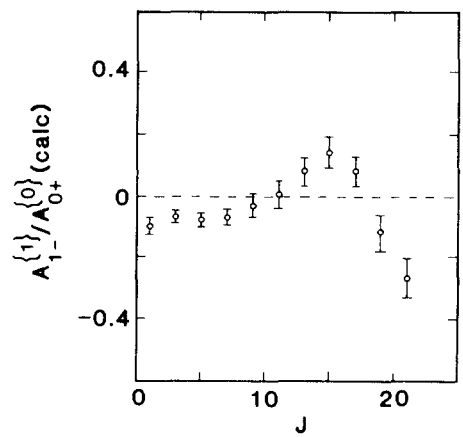

FIG. 7. Calculated $A_1^{\{1\}}$ vs J_i for $E_i = 0.3$ eV, $T_s = 90$ K, T_{rot}(init) $= 0$ K, $\theta_i = 0°$, and $\theta_{exit} = +12°$ to $+15°$. The rotational states were binned as follows (0–2, 2–4, . . . ,20–22). The error bars denote one standard deviation.

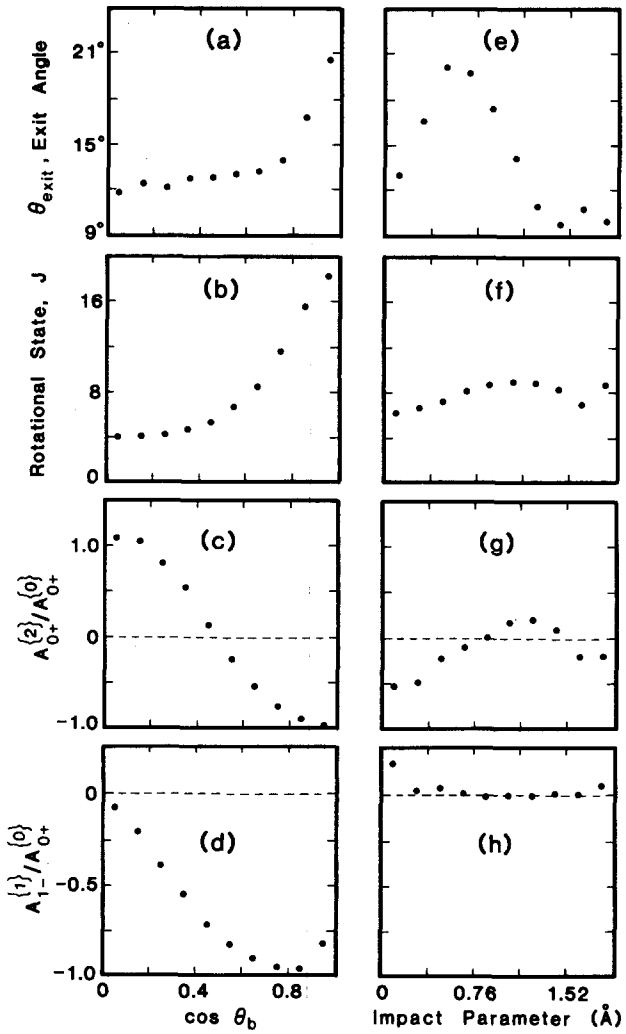

FIG. 8. Calculated parameters of the scattered molecules vs initial conditions for $E_i = 0.3$ eV, $T_s = 90$ K, T_{rot} (init) $= 0$ K, $\theta_i = 0°$. (a) θ_{exit} vs $\cos(\theta_b)$, (b) J vs $\cos(\theta_b)$, (c) $A^{\{2\}}_{0+}$ vs $\cos(\theta_b)$, (d) $A^{\{1\}}_{1-}$ vs $\cos(\theta_b)$, (e) θ_{exit} vs b (Å), (f) J vs b (Å), (g) $A^{\{2\}}_{0+}$ vs b (Å), (h) $A^{\{1\}}_{1-}$ vs b (Å). $\cos(\theta_b) = 0$ corresponds to side-on approach geometry and $\cos(\theta_b) = 1.0$ corresponds to end-on approach geometry. When the impact parameter is zero ($b = 0.0$ Å), then the collision occurs near an atop site, while when b (Å) $= 1.89$ Å then the collision occurs near a hollow site. The $A^{\{2\}}_{0+}$ and $A^{\{1\}}_{1-}$ represent averages over all J weighted according to population.

with initial conditions selected at random with $E_i = 0.3$ eV, $\theta_i = 0°$, T_{rot} (init) $= 0$ K, and $T_s = 90$ K. The dependence of the final properties on initial conditions was monitored by "binning" the trajectories according to the initial conditions. Thus, in Figs. 8(a)–8(d) trajectories were grouped according to the value of the cosine of the angle between the surface normal and the initial direction of the molecular axis, denoted by $\cos(\theta_b)$. For a particular trajectory, if the initial value of this quantity was between 0.0 and 0.1, then the trajectory would be assigned to the first bin, and the final properties would be assigned the value of the median of this bin, 0.05, for the graphing of the final properties in Figs. 8(a)–8(d). For Figs. 8(e)–8(h), the initial impact parameter was taken to be the standard gas-phase meaning of this quantity, defined with respect to the nearest surface atom and binned in increments of 0.189 74 Å.

In Figs. 8(a)–8(d), each bin of molecular orientation geometries represents approximately the same number of trajectories. Conversely, in Figs. 8(e)–8(h) there is a nonuniform distribution of trajectories in the impact parameter bins, with the best statistics for the bins of intermediate impact parameter.

Four final properties are displayed in Fig. 8. The first is the mean value of the final scattering angle with respect to the surface normal [Figs. 8(a) and 8(e)]. The second [Figs. 8(b) and 8(f)] is the mean value of the final rotational angular momentum, expressed in units of $\hbar$; i.e., the mean rotational quantum number, as defined in the Appendix. The third is the mean value of the rotational alignment parameter $A^{\{2\}}_{0+}$ as defined in the Appendix [Figs. 8(c) and 8(g)]. Finally, Figs. 8(d) and 8(h) show the rotational orientation parameter $A^{\{1\}}_{1-}$ as defined in the Appendix.

If we take the z direction to be along the surface normal, then in a normal incidence scattering geometry the x and y directions are not uniquely defined. This does not affect the definitions of the first three final properties discussed above. However, the orientation parameter is defined with respect to the y direction. For Figs. 8(d) and 8(h), we defined the y direction in the most natural ways that allow every trajectory to be included in the statistics. Thus, for Fig. 8(d), we defined the y direction to be the normal to the plane containing the surface normal and the initial molecular bond direction. For Fig. 8(h), we defined the y direction to be the normal to the plane containing the surface normal and the final molecular center-of-mass velocity vector.

Several interesting trends are displayed in Fig. 8. Perhaps the most striking result is the contrast between Figs. 8(d) and 8(h); the final rotational orientation parameter $A^{\{1\}}_{1-}$ is almost completely independent of the impact parameter but depends very strongly on the initial molecular bond direction. In fact, if $\cos(\theta_b) > 0.6$ then $A^{\{1\}}_{1-} < -0.8$. Thus, orientation is almost completely determined by the direction of the bond axis at impact.

Rotational alignment is also a strong function of the initial molecular geometry. Figure 8(c) shows that molecules that approach the surface with a side-on approach geometry, i.e., $\cos(\theta_b)$ near zero, depart with a helicoptering motion ($A^{\{2\}}_{0+} \gg 0$). Conversely, molecules that approach the surface with nearly end-on approach geometry depart with a cartwheeling-type rotation $A^{\{2\}}_{0+} \ll 0$).

The total rotational angular momentum is strongly dependent on the initial molecular geometry as well. Molecules which approach the surface with side-on approach geometry are only weakly rotationally excited on impact, as shown in Fig. 8(b). Much higher rotational excitation results for molecules with more nearly end-on approach geometries. Note that the molecules assigned to the bin with $\cos(\theta_b)$ between 0.9 and 1.0 have a mean initial bond angle of about 17 deg with respect to the surface normal; i.e., very few are virtually perpendicular.

Total J, alignment, and orientation all depend relatively weakly on initial impact parameter, whereas the final scattering angle is a strong function of the impact parameter. Thus, the hypothesis stated in the Introduction, that the effects of initial molecular geometry and impact parameter

can be approximately distinguished in normal incidence scattering, is borne out by the calculations. The only behavior that appears to contradict this is that the final scattering angle depends primarily on the two-dimensional impact parameter, but it is also significantly influenced by the initial molecular geometry; see Fig 8(a). However, the dependence of the final scattering angle on initial molecular geometry results from the dependence of rotational angular momentum excitation upon molecular orientation geometry. Large rotational angular momentum implies a large loss of translational energy into rotation. This loss of energy is mainly from the (local) normal component of the translational energy and thus results in scattering into larger, more grazing, exit angles. Thus, the dependence of scattering angle on initial molecular geometry is a consequence of rotational excitation.

V. SUMMARY

We have carried out measurements of normal incidence scattering of N_2 from cold Ag(111) in order to elucidate the extent to which final scattering angle, rotational state, and rotational polarization are preferentially determined by the dominant initial conditions: the two-dimensional impact parameter and the molecular orientation geometry. Rotational orientation is found to be zero for molecules backscattered along the surface normal and for all molecules integrated over all final scattering angles, as required by symmetry. However, we observe nonzero rotational orientation for molecules scattered away from the normal, and the observed orientation is strong and exhibits a large dependence upon final rotational state. Stochastic classical trajectory simulations satisfactorily reproduce the experimental results. Examination of the calculated trajectories confirms that the final rotational properties are determined predominantly by the initial molecular orientation geometry which is strongly correlated with the direction of the bond axis as the molecule impacts the surface. In contrast, the final scattering angle is determined largely by the two-dimensional impact parameter, which is strongly correlated with the impact site on the surface. There is also an indirect dependence on the molecular orientation geometry through the correlation between scattering angle and final rotational energy.

ACKNOWLEDGMENT

This work was supported by the Office of Naval Research under N00014-87-K-0265.

APPENDIX

The stochastic trajectory method for simulating gas–surface interactions has been described elsewhere.[10] For the present application, the Ag(111) surface was represented by two 4×4 layer slabs of moving silver atoms with periodic boundary conditions imposed in the plane of the surface (the x and y directions) and a third 4×4 layer slab of fixed atoms placed below the moving slabs to provide a template.

Markovian friction and white noise random forces were applied to the second layer of atoms in the direction of the surface normal (z) to account for energy flow into and out of the bulk. For the N_2 collision energies considered here, $E_i < 1$ eV, the 32 moving atoms provided a large enough heat bath that memory effects in the stochastic forces were not significant. In fact, for the conditions considered, stochastic forces are not needed, but the inclusion of frictions and random forces is computationally inexpensive and provides a convenient way to control and maintain the surface temperature. The equilibrium positions of the Ag atoms were taken to be the bulk-terminated positions.

Pairwise additive harmonic forces were assumed for the surface atoms, with first and second neighbor force constants taken to be 1.575×10^{-4} and 0.370×10^{-4} g s^{-2}. The friction constant experienced by each second layer atom was chosen to be 1.54×10^{13} s^{-1}, using the simple prescription proposed by Adelman and Doll.[12] This choice of parameters produces a bulk Debye temperature of about 225 K and a surface normal Debye temperature of about 105 K, which is in accord with experiment.[13]

The internuclear separation of the N_2 molecule was fixed throughout the calculation at its equilibrium value of 1.094 Å. The gas–surface interaction potential was taken to be a pairwise sum of Morse potentials:

$$V=\sum_{i=1}^{2}\sum_{j=1}^{32} D\{\exp[-2\alpha(r_{ij}-r_0)] - 2\exp[-\alpha(r_{ij}-r_0)]\}, \quad \text{(A1)}$$

where r_{ij} is the distance between the nitrogen atom i and the silver atom j. A Morse potential was used in place of the Lennard-Jones interactions employed in some of our previous trajectory studies[14] because the repulsive wall of the latter was found to be somewhat too steep, producing too much rotational excitation. The parameter r_0 primarily controls the corrugation of the gas–surface interaction potential. It was chosen to be $r_0 = 3.8$ Å in order to produce qualitative agreement with experimental angular scattering distributions.[14,15] The binding energy D and the range α were taken to be 0.0052 eV and 1.2 Å^{-1}, respectively, in order to achieve a reasonable molecular–surface binding energy of 0.069 eV, and a reasonable description of the overall rotational energy distribution, as shown elsewhere.[11] Experimental results for rotational alignment and orientation were not used in assigning the potential parameters. In fact, when scaled by the overall rotational energy transfer, the rotational polarization was found to be relatively insensitive to the Morse parameters.

Each trajectory describing an individual encounter of an N_2 molecule with the clean Ag(111) surface was integrated numerically, using an algorithm described previously.[16] Each trajectory commenced with the N_2 molecule a distance (z) 8 Å from the surface plane and with initial x and y positions chosen from a uniform random distribution covering the surface slab. The initial direction of the molecular axis was also chosen randomly. The initial rotational angular momentum was assigned at random from a Boltzmann distribution at the assumed initial (molecular beam) rotational temperature. However, since the experimental mean rotational energy of the incident N_2 molecules was quite low (<20 K), most of the simulations were carried out for zero initial rotational energy. The initial center of mass transla-

tional energy of the N_2 molecules was chosen to be monoenergetic, with speed and direction chosen to match a particular experimental condition.

Initial positions and momenta of the surface atoms were selected for each trajectory at random from a Boltzmann distribution at the surface temperature. The random forces at each integration step were selected from a Gaussian distribution as described elsewhere.[16] Each trajectory was integrated either until the N_2 molecule escaped from the surface to a distance of 8 Å, or for 4000 integrations steps (corresponding to 4×10^{-12} s for the integration time step of 10^{-15} s employed). In no case did the latter undetermined trajectories comprise more than 1% of the total. Consequently, they were neglected in the analysis. From 10 000 to 40 000 trajectories were integrated for each set of conditions examined. Final properties of the scattered molecules were analyzed by strict classical mechanics. Specifically, the following expressions were used to calculate the rotational properties of the scattered molecules:

$$E_r = L^2/2I, \tag{A2}$$

$$A_{1-}^{\{1\}} = L_y/L, \tag{A3}$$

$$A_{1-}^{\{3\}} = (3/8)^{1/2}L_y\left[5L_z^2/(L^2-1)\right]/L, \tag{A4}$$

$$A_{0+}^{\{2\}} = (3L_z^2/L^2) - 1, \tag{A5}$$

$$A_{0+}^{\{4\}} = (1/8)(3 - 30L_z^2/L^2 + 35L_z^4/L^4), \tag{A6}$$

where I is the moment of inertia of the molecule, and L_x, L_y, and L_z are the components of the rotational angular momentum of the scattered molecule, and

$$L^2 = L_x^2 + L_y^2 + L_z^2. \tag{A7}$$

The rotational "quantum number" J was assigned by the prescription

$$J = L/\hbar. \tag{A8}$$

Equations (A2)–(A8) define properties of an individual trajectory. Average values of these quantities for a particular range of scattering angles θ_{exit} were computed by averaging over all trajectories with L and θ_{exit} in the assigned ranges, weighted by the inverse of their center of mass velocity. The inverse velocity weighting corresponds to density detection, not flux, as appropriate for the laser detection scheme employed in these experiments.

The above definitions of the alignment and orientation moments were employed for direct comparision with the experimentally determined $A_{q\pm}^{\{k\}}$ (app)/$A_{0+}^{\{0\}}$ (app). In this paper only measurements of $A_{1-}^{\{1\}}/A_{0+}^{\{0\}}$ (app) are reported. Since in our calculations $A_{0+}^{\{0\}}$ (app) and $A_{0+}^{\{0\}}$ are equal to within a few percent, it is reasonable to compare measured $A_{1-}^{\{1\}}/A_{0+}^{\{0\}}$ (app) directly with calculated $A_{1-}^{\{1\}}$. For the alignment moments, we calculated the real moment $A_{0+}^{\{2\}}$ because it has a more intuitive definition than the corresponding apparent moment.

[1] G. O. Sitz, A. C. Kummel, and R. N. Zare, J. Vac. Sci. Technol. A **5**, 513 (1987).
[2] G. O. Sitz, A. C. Kummel, and R. N. Zare, J. Chem. Phys. **87**, 3247 (1987).
[3] G. O. Sitz, A. C. Kummel, and R. N. Zare, J. Chem. Phys. **89**, 2558 (1988).
[4] G. O. Sitz, A. C. Kummel, R. N. Zare, and J. C. Tully, J. Chem. Phys. **89**, 2572 (1988).
[5] A. C. Luntz, A. W. Kleyn, and D. J. Auerbach, Phys. Rev. B **25**, 4273 (1982); A. W. Kleyn, A. C. Luntz, and D. J. Auerbach, Surf. Sci. **117**, 33 (1982); **152/153**, 99 (1985).
[6] D. C. Jacobs, K. W. Kolasinski, R. J. Madix, and R. N. Zare, J. Chem. Phys. **87**, 5038 (1987).
[7] L. V. Novakoski and G. M. McClelland, Phys. Rev. Lett. **59**, 1259 (1987).
[8] B. D. Kay and T. D. Raymond, Chem. Phys. Lett. **130**, 79 (1986); J. Chem. Phys. **85**, 4140 (1986).
[9] A. C. Kummel, G. O. Sitz, and R. N. Zare, J. Chem. Phys. **88**, 7357 (1988).
[10] J. C. Tully, J. Chem. Phys. **73**, 1975 (1980); J. C. Tully, in *Many Body Phenomena at Surfaces*, edited by D. Langreth and H. Suhl (Academic, New York, 1984), p. 377; C. W. Muhlhausen, L. H. Williams, and J. C. Tully, J. Chem. Phys. **83**, 2594 (1985).
[11] A. C. Kummel, G. O. Sitz, R. N. Zare, and J. C. Tully (in preparation) (paper IV in this series).
[12] S. Adelman and J. D. Doll, J. Chem. Phys. **64**, 2375 (1976).
[13] G. A. Somorjai, *Principles of Surface Chemistry* (Prentice-Hall, Englewood Cliffs, NJ, 1972), p. 99.
[14] C. W. Muhlhausen, J. A. Serri, J. C. Tully, G. E. Becker, and M. J. Cardillo, Isr. J. Chem. **22**, 315 (1982).
[15] H. Asada, Jpn. J. Appl. Phys. **20**, 527 (1981).
[16] J. C. Tully, G. H. Gilmer, and M. Shugard, J. Chem. Phys. **71**, 1630 (1979).